CHAPTER 3

SINGLE MODE TIME INDEPENDENT ANALYSIS OF GYRO-TWT AMPLIFIER

3.1. Introduction

In recent years, considerable attempts have been made in developing gyro-devices, like, gyrotrons, gyro TWTs, gyroklystrons, etc., which belong to the fast-wave group of microwave tube family. These fast wave devices utilize a periodic helical electron beam in a smooth wall interaction structure supporting a fast waveguide mode. The basic operating principle of such a device is based on the electron cyclotron resonance maser (ECRM) instability that allows for large radial dimensions of the RF interaction structure, operation at higher mode of the waveguide and beam cyclotron harmonic modes making the generation or amplification to produce high powers even at the millimeter wave frequencies using reasonable values of magnetic fields. Amongst the gyro-devices, gyrotron, which is a fixed frequency high power source in the millimeter and sub-millimeter frequency range, has been thoroughly studied and being matured, both analytically and experimentally during the last few decades due to its application, mainly in plasma heating for fusion processes. Therefore, the significant concepts of other gyro-devices, like, gyroklystrons, gyroTWTs, and gyrotwystrons have been derived from those of the gyrotrons [Granatstein and Park (1983), Symons *et al.* (1981), Flyagin and Nusinovich (1988)].

Gyro-TWT, an amplifier of this family, is also emerging as one of the promising candidate due to its capabilities to provide high power and broad bandwidth in the millimetre and sub-millimetre wave regime [Barker and Schamiloglu (2001), Nusinovich (2004)]. In the family of gyro-devices, the gyro-TWT amplifier still at the developmental stage, and needs focused efforts both in theory and practice, even though they have undergone three decades of development, yet they are much behind gyrotron oscillators in achievement and not reached to the status of a matured device.

Theoretical research led to the considerable physical insight into the principle of operation of a gyro-TWT amplifier [Granatstein *et al.* (1975), Chu *et al.* (1979), Lau *et al.* (1981), Chu and Lin (1988)]. Some of the milestones in the understanding of this principle are: the development of the nonlinear single mode, single-particle analysis [Nusinovich and Li (1992)], the application of the kinetic theory for a planar configuration, the application of the kinetic theory to the TE mode interaction in a circular waveguide, the stability analysis [Nusinovich and Li (1992)], and the development of a nonlinear self-consistent simulation code for the device in a cylindrical waveguide [Ganguly and Ahn (1982), Chu *et al*. (1980), Nusinovich and Li (1992)].

Since, in a gyro-TWT amplifier the operating frequency of the device is directly proportional to strength of the external magnetic field. Therefore, it requires high magnetic field for its operation at fundamental mode. The requirement of magnetic field further increases with frequency due to which the device cannot be significantly operated at fundamental mode in higher frequency bands such as W-band. As, at such higher frequencies both the cost and size of the device increases in attaining such higher magnetic field strength through superconducting magnets. The requirement of high background magnetic field can be reduced by high harmonic operation of the device. Also, the cyclotron harmonic interactions are, weaker due to reduced beam to mode coupling strength and therefore allow operation of the device at higher levels of beam current. Hence, a harmonic gyro-TWT can significantly operated at higher RF output power than a fundamental gyro-TWT [Furuno *et al.* (1989,) Wang *et al.* (1992), Kou *et al.* (1992), Wang *et al.* (1996), Chong *et al.* (1996), McDermott *et al.* (1998), Wang *et al.* (2000)]. However, at high harmonic operation, the multimode study is very much needed due to the densed

mode spectrum which causes the increase in the parasitic oscillations from the nearby competing modes and lower harmonic modes. The multimode approach is successfully used for gyrotron in the past by many authors to predict accurate power and efficiency which incorporates the effect of presence of all nearby modes inside the RF interaction structure [Vomvoridis (1982), Fliflet *et al.* (1991)]. For gyro-TWT significant amount of work is not available in the literature for studying its multimode behavior. The work reported in the literature to demonstrate the design and analysis for the gyro-TWT's is mainly described by using kinetic theory and single particle, single mode analysis [Nusinovich (1992)].

In the kinetic theory approach, electron beam is described by a distribution function. The distribution function is analogous to a density function depending on space, time and momentum [Chu and Lin (1988)]. Vlasov equation is used to obtain the perturbed electron distribution in the presence of electromagnetic wave. These perturbations are linearized to obtain analytical results.

To analyse the interaction mechanism in the single particle analysis, a representative ensemble of macroparticles is chosen and the evolution of each representative macroelectron is observed in the presence of electromagnetic wave and the background magnetic field. All the representative electrons determine the energy exchange phenomena in beam wave interaction. This analysis also incorporates the single mode consideration for interaction mechanism [Wang *et al.* 2014].

Gyro devices are increasingly designed to operate in high frequency regime for both CW and pulsed peak power. For this, it is necessary to operate at higher order mode and use an oversized interaction structure which obviously increases the density of modes. This

high mode density and switching into parasitic modes affects the performance of the device, such as, efficiency and available operating modes. For these devices multimode analysis is used to predict accurate power and efficiency. In the nonlinear (single particle) analysis, one do not take account mode competition by nearby modes. The multimode analysis, the effect of competing mode is studied using fully nonlinear formulation. These types of studies are mainly reported for the gyrotron oscillators [Vomvoridis (1982), Fliflet *et al.* (1991)]. Therefore, in the present chapter time independent single mode analysis of a gyro-TWT amplifier is carried out in detail. For the benchmarking selected fundamental mode, 92GHz, experimental gyro-TWT amplifier has been carried out and validated against the single mode time independent analysis and reported experimental results in the literature [Song *et al.* 2004].

3.2. Description of CRM Interaction

CRM interaction occurs when a hollow annular electron beam propagate in a magnetic field. The presence of the DC axial magnetic field induces gyrations in the electron orbits. A schematic diagram of gyro-TWT show in Figure in 3.1.The electron beam's longitudinal velocity v_z, a transverse velocity v_t, Larmor radius r_L, and the relativistic mass factor

$$\gamma = \frac{1}{\sqrt{1-\left(\frac{v_t^2+v_z^2}{c^2}\right)}} \tag{3.1}$$

The relativistic cyclotron frequency

$$\Omega_r = \frac{eB_0}{\gamma m_0} \tag{3.2}$$

and Larmor radius

$$r_L = \frac{v_t}{\Omega_r} \tag{3.3}$$

where B_0 is the axial DC magnetic field, e and m_0 are the magnitude of the charge and rest mass of the electron, respectively [Sirigiri (1999)]. For explain the phase bunching the Larmor radii of the electrons in the phase space as a function of time. Such trajectories of 128 numbers of electrons in a single beamlet under the influence of RF fields are shown in Figures 3.2. The figures are normalized $x-y$ plots with respect to the direction of the local electric field.

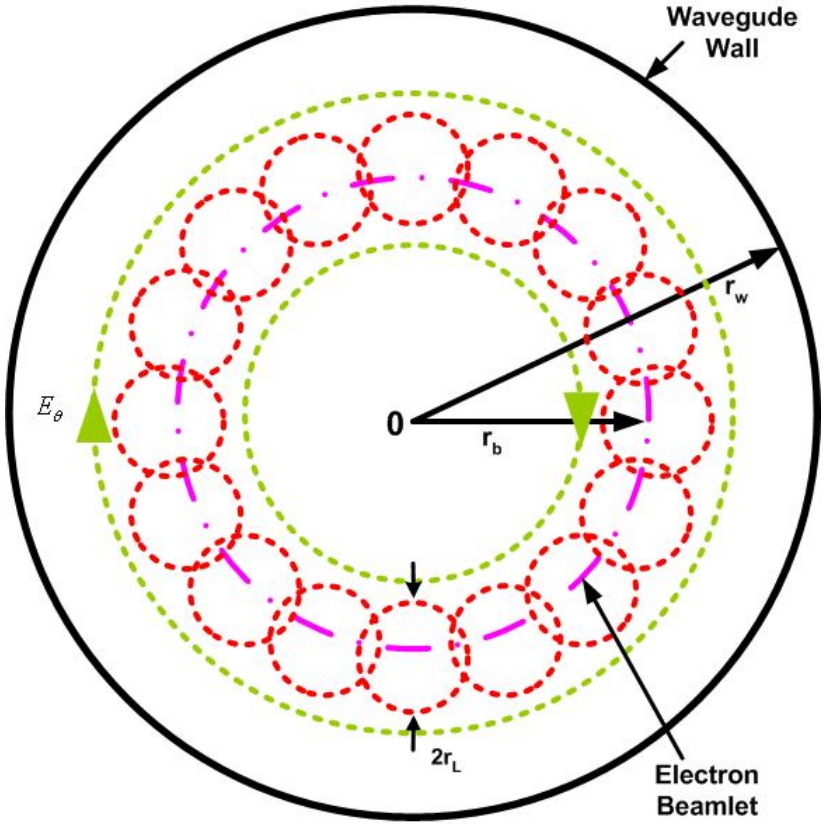

Figure 3.1. Schematic of TE_{0n} mode RF electric field in a waveguide with the electron beamlets.

The cyclotron frequency of an electron is inversely proportional to its relativistic mass γm_0 those electrons which gained energy will gyrate slower while the others lost energy gyrate faster. Initally electrons bunch to form at the phase position of the electron field and then drift leg in phase for energy extraction. This can be achieved when the frequency of the RF wave slightly higher than the cyclotron frequency of the electrons. The magnetic tuning is important factor that would produce exact synchronism between the transverse electric field and the cyclotron motion of the electrons. After the extraction of energy the electrons lose synchronism with the RF wave and finally enter the accelerating phase thus extracting energy from the RF wave showing saturation of the interation. For enhencing the coupling of electron beam usually cylindrical waveguide is used as amplifier and oscillator.

3.3. Kinetic Theory

3.3.1. Linear Dispersion Relation

The beam-wave interaction mechanism in gyro-TWT devices is simply understood as the coupling between the electromagnetic waveguide mode and the beam cyclotron harmonic modes. The combined dispersion relation which is the product of the waveguide mode dispersion and the beam cyclotron mode dispersion relations coupled by the source term namely, the normalized electron beam current [Sirigiri (1999)]. The operating characteristic of any vacuum electron devices is governed by the dispersion relation and device synchronism between an EM mode and a fast electron cyclotron mode. This can be obtained at the grazing intersection between the beam mode and waveguide mode dispersion curve. An electron beam can support a space charge mode, and a number of electromagnetic modes based on the geometry of the interaction circuit. Based on the

nature of interaction of fast waveguide mode with electron beam, a device could either be an oscillator or an amplifier.

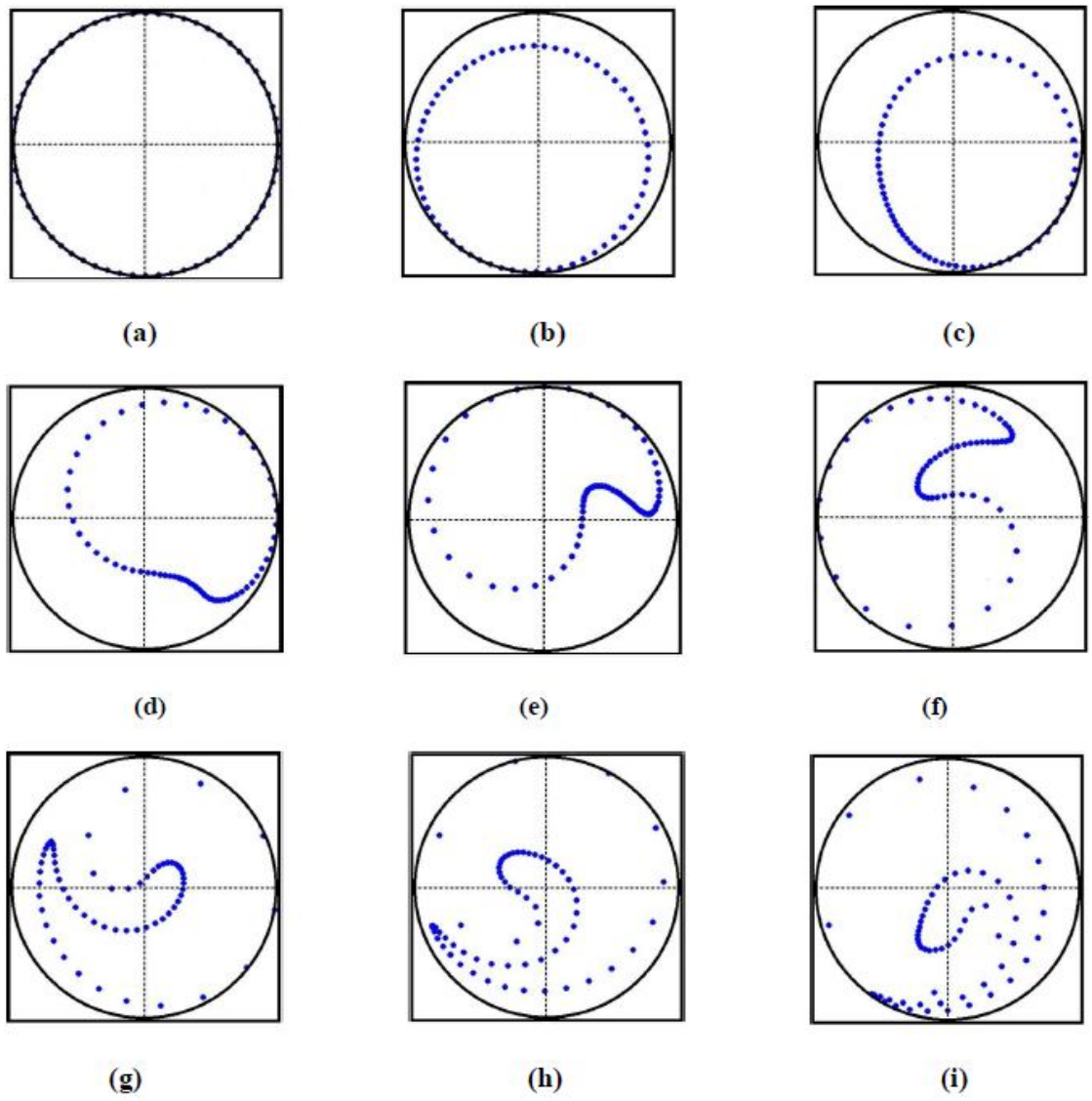

Figure 3.2. Phase distribution of electron by ●. The initial phase distribution is shown by ○

Beam-mode dispersion relation

The beam mode dispersion relation of gyrotron devices can be obtained using the concept that over a cyclotron period, one or more RF cycles are completed [Basu (1996)].

$$\omega - k_z v_z - s\Omega/\gamma \cong 0 \tag{3.4}$$

The equation (2.5) is popularly known as the beam-mode dispersion equation.

Waveguide-mode dispersion relation

The azimuthal electric field components can be written as

$$E_\theta = \left(\frac{j\omega\mu_0}{\gamma_n} \right) H_{z0}\, J'_m(\gamma_n r)\, \exp j\left(\omega t - k_z z - m\theta\right) \tag{3.5}$$

For the perfectly conducting waveguide wall, the azimuthal component of electric field intensity would be null at the metal wall, i.e., $E_\theta = 0$ at $r = r_w$. Consequently, Bessel derivative must be zero. Hence,

$$J'_m(\gamma_n r) = 0 \tag{3.6}$$

and which gives

$$\omega^2 - k_z{}^2 c^2 - \omega_c^2 = 0 \tag{3.7}$$

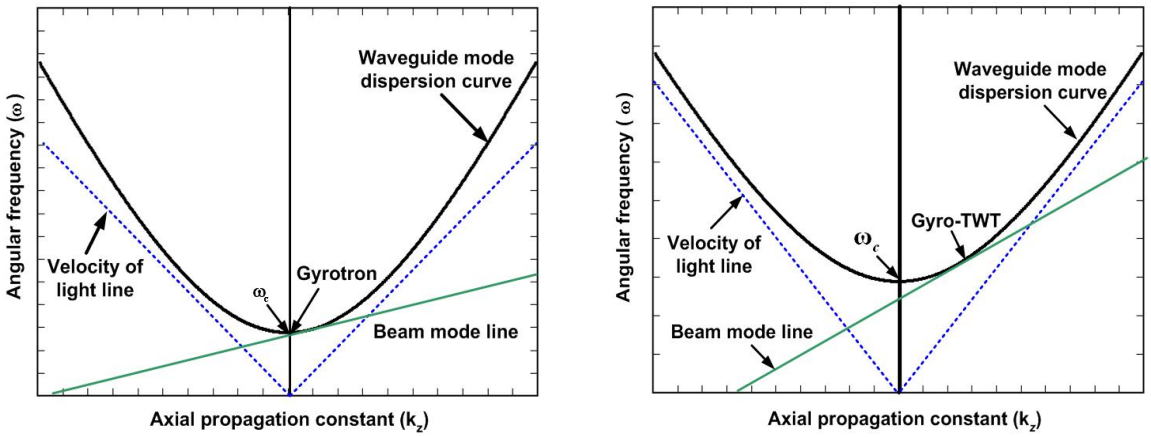

Figure 3.3. Dispersion diagrams showing the operating regions of interaction for (a) gyrotron, and (b) gyro-TWT.

The dispersion relations for various gyro devices are shown in Figure 3.3(a) and (b) and that provide the information about the operating conditions of various gyrotron amplifiers and oscillators.

Kinetic Approach

There are two ways to derive linear dispersion relation of CRM system. In kinetic approach, solving the relativistic Vlasov's equation to obtain the perturbed electron distribution function. Second by linearizing the single-particle equations of motion in the small-signal limit to obtain a dispersion relation [Sirigiri (1999)]. Without velocity spread and simple structure kinetic theory approach is follow. On the other hand derivation of the single particle equations of motion for an arbitrary shape of the waveguide is much easier.

Dispersion relation from kinetic theory

The transverse component of TE mode may be expressed as

$$\vec{\mathrm{E}}_{\mathrm{t}}(\vec{r},t) = \mathrm{Re}\left\{\Pi(z)\ \vec{e}(\vec{r})\exp(-i\omega t)\right\} \tag{3.8}$$

$$\vec{\mathrm{B}}_{\mathrm{t}}(\vec{r},t) = \mathrm{Re}\left\{\Upsilon(z)\ \vec{\mathrm{b}}(\vec{r})\exp(-i\omega t)\right\} \tag{3.9}$$

where $\vec{\mathrm{b}}(\vec{r})$ and $\vec{e}(\vec{r})$ are the unit transverse vector functions given by

$$\vec{b}\left(\vec{r}\right) = -\nabla_t \Psi \tag{3.10}$$

$$\vec{e}\left(\vec{r}\right) = \hat{z}\times\nabla_t \Psi, \tag{3.11}$$

The scalar function Ψ, satisfies the Helmholtz wave equation

$$(\nabla_t^2 + \mathrm{k}_t^2)\Psi = 0 \tag{3.12}$$

and the boundary condition

$$\frac{d\Psi}{dn} = 0, \tag{3.13}$$

at the waveguide wall. k_t denotes the transverse wave-number and $\partial / \partial n$ denotes the norma derivative [Fliflet (1986)]. The vector functions satisfy the orthonormality condition when integrated over the waveguide cross-section

$$\int_S dS \ \vec{h}_i . \vec{h}_j = \delta_{ij,} \tag{3.14}$$

where $\vec{h}$ denotes either $\vec{e}(\vec{r})$ or $\vec{b}(\vec{r})$ and the Kronecker delta function

$$\delta_{ij} = 1 \qquad \text{if} \quad i = j, \quad \delta_{ij} = 0 \qquad \text{if} \quad i \neq j \tag{3.15}$$

The axial field components are given by

$$B_z = \mathrm{Re}\left\{ i\left(k_t^2 / \omega\right) \Pi(\mathrm{z}) \Psi \exp(-i\omega t) \right\} \tag{3.16}$$

The axial profile functions $\Pi(z)$ and $\Upsilon(z)$ are related according to

$$\Upsilon(\mathrm{z}) = -\left(\mathrm{i}/\omega\right)\left(d\Pi(z)/dz\right) \tag{3.17}$$

In case of a circular waveguide, the scalar function Ψ is given by

$$\Psi_t(r) = \mathrm{C}_{mn} \mathrm{J}_m(\mathrm{k}_t\, r) \exp(im\theta) \tag{3.18}$$

where, J_m is a Bessel function of the first kind and $k_t = v_{mn} / r_w$, v_{mn} is the nth zero of J'_m and r_w is the waveguide wall radius. The normalization constant is given by

$$C_{mn} = \left\{ \sqrt{\pi (v_{mn}^2 - m^2)}\ \mathrm{J}_m\left(v_{mn}\right) \right\}^{-1} \tag{3.19}$$

Using the above formulation and considering only the forwarded propagation wave $\Pi(z) = \Pi_0 \exp(ik_z z),$ we can express the RF field components as

$$B_z = \mathrm{Re}\left\{ i\left(k_t^2 / \omega\right) \Pi_0 C_{mn} J_m(\mathrm{k}_t\, r)\, \mathrm{e}^{-\mathrm{i}\left(\omega t - k_z z - m\theta\right)} \right\} \tag{3.20}$$

$$B_r = \mathrm{Re}\left\{ -\left(k_t k_z / \omega\right) \Pi_0 C_{mn} J'_m(\mathrm{k}_t\, r)\, \mathrm{e}^{-\mathrm{i}\left(\omega t - k_z z - m\theta\right)} \right\} \tag{3.21}$$

$$B_\theta = \mathrm{Re}\left\{-i\left(mk_z/r\omega\right)\Pi_0 C_{mn} J_m(\mathrm{k}_t\, r)\,\mathrm{e}^{-\mathrm{i}(\omega t - k_z z - m\theta)}\right\} \tag{3.22}$$

$$E_r = \mathrm{Re}\left\{-i\left(m/r\right)\Pi_0 C_{mn} J_m(\mathrm{k}_t\, r)\,\mathrm{e}^{-\mathrm{i}(\omega t - k_z z - m\theta)}\right\} \tag{3.23}$$

$$E_\theta = \mathrm{Re}\left\{k_t \Pi_0 C_{mn} J'_m(\mathrm{k}_t\, r)\,\mathrm{e}^{-\mathrm{i}(\omega t - k_z z - m\theta)}\right\} \tag{3.24}$$

$$E_z = 0 \tag{3.25}$$

where, k_z is the axial propagation constant, μ_o is the permeability of free space and m is the azimuthal harmonic number.

Electron Beam Dynamics

The dynamics of the electron beam is described by the relativistic Vlasov equation

$$\left(\frac{\partial}{\partial t} + \frac{\vec{p}}{\gamma m_{e0}}.\nabla - e\left\{\vec{E} + \vec{v}\times(\mathrm{B}_0\,\hat{z} + \vec{\mathrm{B}})\right\}.\nabla p\right) f(\vec{\mathrm{r}},\vec{\mathrm{p}},\mathrm{t}) = 0, \tag{3.26}$$

Where $f(\vec{\mathrm{r}},\vec{\mathrm{p}},\mathrm{t})$ is the electron distribution in the momentum space, ∇ denotes the gradient in configuration space and ∇p is the gradient in the momentum space.

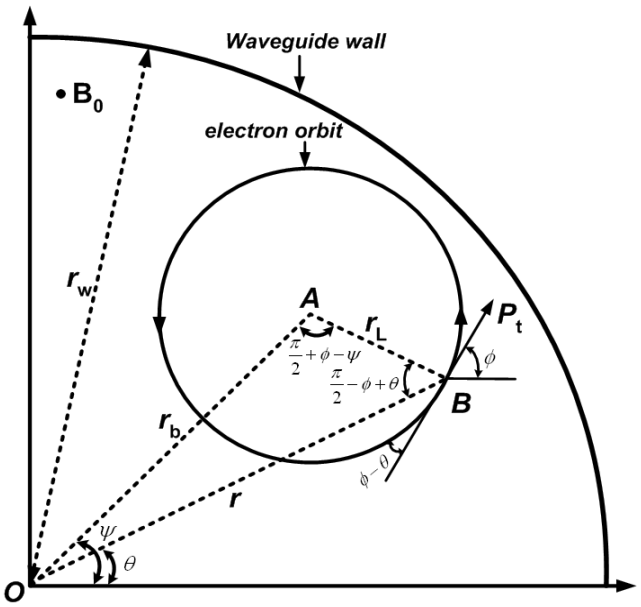

Figure 3.4. Projected electron orbit (circle) based on the instantaneous position and velocity of the electron at point B in the presence of uniform magnetic field.

The Figure 3.4 shows the cross section of the interaction circuit with the co-ordinate system, which is considered in the present analysis. In a weak beam-wave coupling system, the real part of the axial propagation constant should be in the vicinity of the axial propagation constant of the beam absent interaction circuit. Further, space charge effect is neglected. The detailed explanation of the dispersion relation based on the kinetic approach has been narrated by [Chu and Lin (1988), Fliflet (1986), Sirigiri (1999)]. Accordingly, the dispersion relation is expressed as

$$D(\omega,k_z)=\left(\frac{\omega}{c}\right)^2-k_z^2-k_{mn}^2\left\{1-(1+i)\left(1+\frac{m^2}{x_{mn}^2-m^2}\frac{\omega^2}{\omega_c^2}\right)\frac{\delta}{r_w}\right\}+\frac{2e^2\mu_0}{m_{e0}\pi r_w^2 K_{mn}}\int_0^{r_b^{max}} r_b\,dr_b\int_{p_t=0}^{\infty} p_t\,dp_t$$

$$\int_{p_z=-\infty}^{\infty} dp_z\sigma_0 h_b(r_b)\,g(p_t,p_z)\left[\frac{\left(\omega^2-k_z^2c^2\right)p_t^2 H_{-s,m}}{\gamma^3 m_{eo}^2c^2\left(\omega-k_zv_z-s\frac{\Omega}{\gamma}\right)^2}-\frac{(\omega-k_zv_z)Q_{-s,m}-k_tv_tU_{-s,m}}{\gamma\left(\omega-k_zv_z-s\frac{\Omega}{\gamma}\right)}\right]$$

$$=0 \tag{3.27}$$

where, 'δ' is the skin depth of the circuit wall, ω_c is the cut-off frequency of the lossless interaction circuit, p_t and p_t are transverse and axial momentum of electrons, respectively, σ_0 is the number of electrons per unit volume, $h_b(r_b)$ is the distribution of electrons in the radial direction and $g(p_t,p_z)$ represents the distribution of the electrons in the momentum space. The other quantities are defined as

$$K_{mn}=\left(1-\frac{m^2}{v_{mn}^2}\right)J_m^2(v_{mn}) \tag{3.28}$$

$$H_{-s,m}=J_{s-m}^2(k_tr_g)\,J_s'^2(k_tr_L) \tag{3.29}$$

$$Q_{-s,m} = 2H_{-s,m} + \left(k_t r_L\right) J_s'\left(k_t r_L\right)\left\{2J_{s-m}^2\left(k_t r_g\right) J_s''\left(k_t r_L\right) - J_s(k_t r_L)\left[\frac{1}{k_t r_g} J_{s-m}\left(k_t r_g\right)\right.\right.$$

$$\left.\left. J_{s-m}'\left(k_t r_g\right) + J_{s-m}'^2\left(k_t r_g\right) + J_{s-m}\left(k_t r_g\right) J_{s-m}''\left(k_t r_g\right)\right]\right\} \tag{3.30}$$

A spread in the axial momentum of the beam causes variation in the resonance condition equation (3.27), thereby deteriorating the interaction. For a gyro-TWT amplifier under the simplest case, the distribution function of the electron beam can be represented as

$$h\left(r_b\right) = A_b \frac{1}{r_b} \delta\left(r_b - r_{b0}\right) \tag{3.31}$$

$$g\left(p_t, p_z\right) = \frac{1}{2\pi p_t} \delta\left(p_t - p_{t0}\right) \delta\left(p_z - p_{z0}\right) \tag{3.32}$$

The operating beam current I_0 flows through the cross-section of the interaction circuit is expressed as

$$I_0 = \sigma_0 A_b e v_z \tag{3.33}$$

Substituting equations (3.31) and (3.32) into equation (3.27), and using equation (3.33) to integrate over the momentum space, we get the dispersion for a gyro-TWT amplifier as

$$D\left(\omega, k_z\right) = \left(\frac{\omega}{c}\right)^2 - k_z^2 - k_t^2\left[1 - \left(1+i\right)\left(1 + \frac{m^2}{v_{mn}^2 - m^2}\frac{\omega^2}{\omega_c^2}\right)\frac{\delta}{r_w}\right] + \frac{e\mu_0}{c m_{e0} \pi r_w^2 K_{mn}} \frac{I_0}{\gamma \beta_z}$$

$$\times\left[\frac{\left(k^2 - k_z^2\right)\beta_t^2 H_{-s,m}}{\left(k - k_z\beta_z - s k_e\right)^2} - \frac{\left(k - k_z\beta_z\right) Q_{-s,m} - k_t \beta_t U_{-s,m}}{\left(k - k_z\beta_z - s k_e\right)}\right] = 0 \tag{3.34}$$

The above dispersion relation can be numerically solved for complex solutions of *k* for real values of ω to obtain the growth rate of the CRM instability [Sirigiri (1999)]. The conditions for the excitation of absolute and convective instabilities can be obtained from methodology developed in [Bers (1983)].

3.4. Single mode Time Independent Analysis

Single Particle Analysis

The nonlinear analysis considered here to study the evolution of electron beam in the background of RF wave supported by the interaction structure and a static axial magnetic field. The analysis includes the drift of the electron guiding centres and the effects of in homogeneity of the magnetic field. The analysis described here is advantageous in many ways. One of the features of the present analysis lies in its validity for all the gyro-TWT operating at arbitrary cyclotron harmonics and any waveguide mode. It is important to maintain synchronism between background magnetic field and the gyrating electrons to enhance the interaction efficiency. This goal can be achieved by tapering of the external magnetic field [Nusinovich and Li (1992)]. The non-uniformity of operating magnetic field can also be included in the present analysis. This analysis describes fully nonlinear behavior of the interaction process and thus can be used to study the saturation effects, the space charge effect are neglected.

3.4.1. Waveguide Excitation Equations

The electromagnetic field expressions in the absence of electron beam can be written in the waveguide centre coordinate as

$$\vec{E} = \mathrm{Re}\left\{ \mathrm{A}\, \vec{E}_s\left(r_t\right) e^{-i\left(\omega t - k_{z,c} z\right)} \right\} \tag{3.35}$$

$$\vec{H} = \mathrm{Re}\left\{ A H_s\left(r_t\right) e^{-i\left(\omega t - k_{z,c} z\right)} \right\} \tag{3.36}$$

where functions $\vec{E}_s$ and $\vec{H}_s$ describe the transverse electric and magnetic fields of the structure, A is the amplitude, r_t is the transverse coordinate and $k_{z,c}$ is the axial propagation constant of the waveguide, in absence of the electron beam. The gyro-TWT

uses cylindrical waveguide as its RF interaction structure and operates in the transverse electric mode. In the presence of electron beam, the electric and magnetic fields can be represented by applying continuity and Maxwell's equation as

$$\vec{E} = \mathrm{Re}\left\{ A(z)\vec{E}_s\left(r_t\right)e^{-i(\omega t - k_z z)} - i\frac{1}{\varepsilon_0 \omega} j_{\omega,z} e^{-i\omega t}\hat{z}_0 \right\} \tag{3.37}$$

$$\vec{H} = \mathrm{Re}\left\{ A(z)\vec{H}_s\left(r_t\right)e^{-i(\omega t - k_z z)} \right\} \tag{3.38}$$

The electron beam can be represented in the current density form as

$$\vec{j} = \mathrm{Re}\left\{ \left(\vec{j}_{\omega,t} + j_{\omega,z}\hat{z}_0 \right) e^{-i\omega t} \right\} \tag{3.39}$$

where, $j_{\omega,z}$ determines the shift in fields due to the presence of electron beam. Now, the complex Fourier amplitudes of the $\vec{E}$ and $\vec{H}$ fields are introduced as $\vec{E}_\omega$ and $\vec{H}_\omega$ respectively [Fliflet (1986)]. Therefore, the field components in terms of E_ω and H_ω can be expressed as

$$\vec{E}_\omega = A\left(z\right)e^{i(\Delta k_z)z}\vec{E}_s' - \frac{i}{\varepsilon_0 \omega} j_{\omega,z}\hat{z}_0 \tag{3.40}$$

$$\vec{H}_\omega = A\left(z\right)e^{i(\Delta k_z)z}\vec{H}_s' \tag{3.41}$$

where $\Delta k_z = k_z - k_{z,c}$, substituting the values of E_ω and H_ω from (3.34) and (3.41) into Maxwell's equations and averaging over the cross-section of former and integrating over the cross section of the interaction circuit gives,

$$\left\{ \frac{d}{dz} + i\left(\Delta k_z\right) \right\} A\left(z\right) = -\frac{1}{N_s}\iint dS_\perp \, \vec{j}_\omega . \vec{E}_s^{\,*} e^{ik_z z} \tag{3.42}$$

where, 'N_s' is the norm factor of the interaction circuit is defined as

$$N_s = \iint dS_\perp \left\{ \left[\vec{E}_s \times \vec{H}_s^* \right] - \left[\vec{H}_s \times \vec{E}_s^* \right] \right\} \hat{z} \tag{3.43}$$

Fourier expansion of the current density $\vec{j}_\omega$ may be written as,

$$\vec{j}_\omega = \frac{1}{\pi}\int_0^{2\pi} \vec{j}_t e^{i\omega t} d(\omega t) \tag{3.44}$$

From Liouville's theorem, the law of conservation of charge for an electron beamlet requires that,

$$dq = j_z\, dt = dq_0 = j_{z0}\, dt_0 \tag{3.45}$$

Using the above law of conservation of charge, the equation (3.42) is rewritten as,

$$\left\{\frac{d}{dz} + i(\Delta k_z)\right\} A(z) = -\frac{1}{N_s}\iint dS_\perp \frac{j_{z0}}{\pi}\left\{\int_0^{2\pi} \frac{\vec{j}_t \cdot \vec{E}_s^*}{j_z} e^{i(\omega t - k_z z)} d(\omega t_0)\right\} \tag{3.46}$$

3.4.2. Electron Beam Dynamic

The primary forces on the electron beam are the accelerating voltage, the axial DC magnetic field and the RF fields. Though the space charge forces on the beam can be comparable to the above mentioned forces in some circumstances, however, in the present case the space charge forces are negligible [Sirigiri (1999)]. In practice, a gyro-TWT amplifier uses a beam current much lower than either the self-limiting or the critical current for the electron beam. Some studies on the effects of space charge fields have indicated that the bunching is enhanced by the space charge fields in a CRM under some circumstances. The various forces on the electron beam can be represented by the Lorentz force equation

$$\frac{d\vec{p}}{dt} = -e\left\{\vec{E} + \vec{v} \times \left(\vec{B}_0 + \vec{B}\right)\right\} \tag{3.47}$$

where $\vec{B}_0 = B_0 \hat{z} - r/2\left(dB_0/dz\right)\hat{r}$ is an linear tapered external magnetic field along the axial direction of the interaction circuit, $\vec{p}$ is the momentum of the electrons, $\vec{E}$, $\vec{B}$ are the electric and magnetic fields, respectively, and $\vec{v}$ is the velocity of the electrons. Using the

normalization quantities $t' = \omega t$, $z' = kz$, $v'_z = v_z / c = \beta_z$, $v'_\perp = v_\perp / c = \beta_\perp$, $\vec{p}' = \vec{p} / m_{e0}c = \gamma mv$, and $\mu = eB_0 / m_{e0}\omega$, the Lorentz force equation is rewritten as

$$\frac{d\vec{p}}{dt} = -e\vec{v} \times \vec{B}_0 + \vec{F} + \vec{R} \tag{3.48}$$

where,

$$\vec{F} = -e\left\{\vec{E} + \vec{v} \times \vec{B}\right\} \tag{3.49}$$

$$\vec{R} = e\left\{\vec{v} \times \frac{1}{2}\frac{dB_0}{dz}\vec{r}\right\} = eB_0 g_t \left(\vec{v} \times \vec{r}\right) \tag{3.50}$$

and

$$g_t = \frac{1}{2B_0}\frac{dB_0}{dz} \tag{3.51}$$

The vectors $\vec{F}$ and $\vec{R}$ are also normalized as

$$\vec{F}' = \frac{\vec{F}}{\omega m_{e0} c} \tag{3.52}$$

$$\vec{R}' = \frac{\vec{R}}{\omega m_{e0} c} = \frac{\mu}{c} g_t \left(\vec{v} \times \vec{r}\right) \tag{3.53}$$

Using the above defined normalized quantities, the normalized Lorentz force equation is given by

$$\frac{d\vec{p}'}{dz'} + \mu\left(\frac{\vec{p}'}{p'_z} \times \hat{z}'\right) = \frac{1}{\beta_z}\left(\vec{F}' + \vec{R}'\right) \tag{3.54}$$

Zero Order Approximation

The electron orbits in the presence of the EM wave are computed as a perturbation to the solution in the absence of RF field. The unperturbed solution is the zero order approximation for the electron orbits. In the absence of the RF field, the forces acting on the electron are the axial DC magnetic field and the accelerating longitudinal DC electric field. Figure 3.5 represents the schematic of the interaction circuit along with the co-

ordinates and for such a system the motion and the position of the gyrating electrons in a homogeneous magnetic field are described as $p'_x = -p_t sin\theta$, $p'_y = p_t cos\theta$, $x' = X' + r'_L cos\theta$,

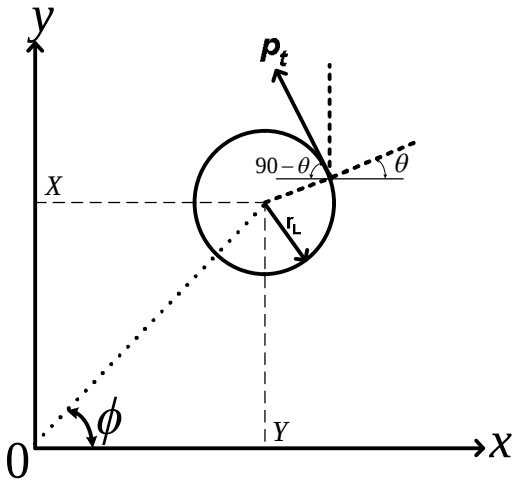

Figure 3.5. A schematic of the interaction circuit with cylindrical coordinate system.

$y' = Y' + r'_L sin\theta$, $\theta = (\mu\tau/\gamma) + \phi$ and $\tau = t - t_0$. Here, t_0 being the entrance time. In the above equations $x' = kx, y' = ky, X' = kX$, $Y' = kY, and\, r'_L = kr_L$ are introduced as normalized quantities. It may be mentioned that in the absence of the RF field r'_L, x', y', X' and Y' are constant. The other conserved quantities in such a situation are p'_z, the electron energy and the relativistic mass factor γ.

Forces due to Magnetic Field Inhomogeneity

The presence of the radial magnetic field components due to the tapered external magnetic field adds new forces on electrons. The external magnetic field will not cause any change in the net electron energy. This is evident from the evolution of the electron energy along the interaction circuit length [Sirigiri (1999)]. The normalized force due to the radial magnetic field given as $\vec{R}'$ in (3.53) is estimated as,

$$\vec{R}' = \frac{\mu}{c} g_t \left(\vec{v} \times \vec{r}\right) = \frac{\mu}{c} g_t \left(-p_t sin\theta \hat{x} + p_t cos\theta \hat{y}\right) \times (x'\hat{x} + y'\hat{y})$$

$$= -g\left(\beta_z \mu r_b sin\phi + \frac{\beta_z \beta_t}{k} sin\theta\right)\hat{x} + g_t\left(\beta_z \mu r_b cos\phi + \frac{\beta_z \beta_t}{k} cos\theta\right)\hat{y}$$

$$-g\left(\beta_z \mu r_b \cos(\phi - \theta) + \frac{\beta_t^2}{k} sin\theta\right)\hat{z} \tag{3.55}$$

Electron Motion in the Presence of RF Fields

In the presence of the EM fields, $F' \neq 0$, and the radial magnetic field equations describing the electron dynamics is written in terms of the perturbation to the zero-order orbits derived in the previous section[Sirigiri (1999)]. The motion of electron in the presence of RF fields is obtained using Vander Pol's method and the new equations for the electron dynamics are given as

$$\dot{p}_t' sin\theta + p_t' \dot{\phi} cos\theta = -\frac{1}{\beta_z}\left(F_x' + R_x'\right) \tag{3.56}$$

$$\dot{p}_t' cos\theta - p_t' \dot{\phi} sin\theta = \frac{1}{\beta_z}\left(F_y' + R_y'\right) \tag{3.57}$$

$$\dot{X}' + \dot{r}_L' cos\theta - r_L' \dot{\psi} sin\theta = 0 \tag{3.58}$$

$$\dot{Y}' + \dot{r}_L' sin\theta - r_L' \dot{\psi} \cos\theta = 0 \tag{3.59}$$

$$\theta = \mu \int_0^z \frac{1}{p'_z} dz' + \phi \tag{3.60}$$

In the above equations, the dots imply derivatives with respect to the normalized distance, *i. e.*, (d/dz'). Also, we have used $\dot{p}_z' = F_z'/\beta_z = 0$. Since, the forces on the electron are azimuthally symmetric with respect to its guiding centre, it is advantageous to

transform the above equations into the polar coordinate form. The transformation is done based on the Figure 3.6 and obtained as

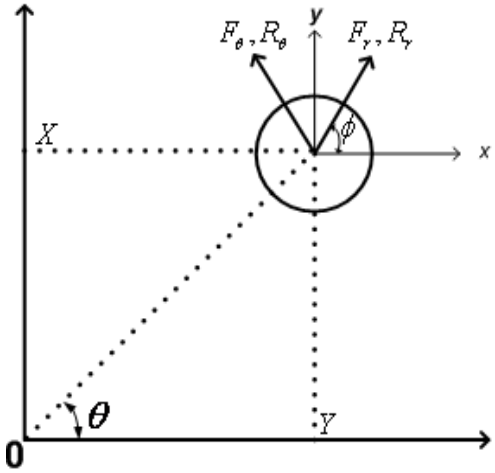

Figure 3.6. The orientation of radial and azimuthal forces on the electron in guiding center coordinates [Sirigiri (1999)].

$$F_r' = F_x' cos\theta + F_y' sin\theta \tag{3.61}$$

$$F_\theta' = -F_x' sin\theta + F_y' cos\,\theta \tag{3.62}$$

$$R_r' = R_x' cos\,\theta + R_y' sin\,\theta \tag{3.63}$$

$$R_\theta' = -R_x' sin\,\theta + R_y' cos\,\theta \tag{3.64}$$

Using the above transformation the equations of motion of electron in the presence of RF fields is given in (3.56) - (3.60) can now be written as

$$\dot{p}_t' = \frac{1}{\beta_z}\left(F_\theta' + R_\theta'\right) \tag{3.65}$$

$$\dot{p}_z' = \frac{1}{\beta_z}\left(F_z' + R_z'\right) \tag{3.66}$$

$$p_t'\dot{\phi} = -\frac{1}{\beta_z}\left(F_r' + R_r'\right) \tag{3.67}$$

$$\dot{X}' = -\frac{1}{\mu\beta_z}\left(F_y' + R_y'\right) \tag{3.68}$$

$$\dot{Y}' = \frac{1}{\mu\beta_z}\left(F_x' + R_x'\right) \tag{3.69}$$

The force $\vec{F}'$ is a periodic function of the angular coordinate θ, hence one may represent it in the form of a sum of infinite azimuthal harmonics as

$$\vec{F}' = \sum_{l=-\infty}^{\infty} \vec{F}_l' e^{il\theta} \tag{3.70}$$

where $$\vec{F}_l' = \frac{1}{2\pi}\int_0^{2\pi} \vec{F}' e^{il\theta} d\theta \tag{3.71}$$

The fields in the interaction circuit can be represented in a form similar to that developed in the previous section as

$$\vec{E} = \mathrm{Re}\left\{A\vec{E}_s\left(r_t\right)e^{-i(\omega t - k_z z)}\right\} \tag{3.72}$$

$$\vec{H} = \mathrm{Re}\left\{A\vec{H}_s\left(r_t\right)e^{-i(\omega t - k_z z)}\right\} \tag{3.73}$$

for a travelling wave circuit. Now the form of $\vec{F}'$ is identified in (3.65) - (3.69) as

$$\vec{F}' = -\mathrm{Re}\left\{\frac{eA}{m_{e0}c\omega}\sum_{l=-\infty}^{\infty}\vec{G}_l e^{i\vartheta_l}\right\} \tag{3.74}$$

where, $$\vec{G} = \vec{E}_s + \vec{v}\times\vec{B}_s \tag{3.75}$$

and $$\vartheta_l = l\theta - \left(\omega t - k_z z\right) \tag{3.76}$$

In order to simplify the analysis, certain mathematical approximations are made and introduced that are physically valid for the gyro-TWT interaction particularly as follows: the condition of cyclotron resonance for a travelling waveguide is given by

$$\left|\omega - k_z v_z - s\frac{\Omega}{\gamma}\right| \ll \omega \tag{3.77}$$

where, '*s*' is the cyclotron harmonic number. The interaction between the electrons and the RF field occurs over many cycles and in one such cycle the variables p_t', p_z', ψ, X' and Y' are assumed to be varying slightly [Sirigiri (1999)]. This time scale of variation over one cyclotron period is called the fast-time scale contrary to slow-time scale variation corresponding to the transit time in the interaction region. With the above assumptions, the equations (3.65) - (3.69) are averaged over the fast gyro-motion and hence obtained the reduced equations in which all the non-resonant harmonics of the periodic force vanish. Also the terms $g\beta_z \mu r_b sin(\phi - \theta)$ and $g\beta_z \mu r_b cos(\phi - \theta)$ occurring in the expressions for $\vec{R}_r'$ and $\vec{R}_\theta'$ vanish due to the averaging over the fast electron gyrations. After averaging, the coupled set of momentum equations are obtained as

$$\dot{p}_t' = -\frac{1}{\beta_z}\mathrm{Re}\left\{A' G_{s\theta} e^{i\vartheta_s}\right\} + g_t \frac{\beta_t}{k} \tag{3.78}$$

$$\dot{p}_z' = -\frac{1}{\beta_z}\mathrm{Re}\left\{A' G_{sz} e^{i\vartheta_s}\right\} - g_t \frac{\beta_t^2}{k\beta_z} \tag{3.79}$$

$$p_t'\left[s\frac{\mu}{p_z'} - \frac{1}{\beta_z} - \dot{\vartheta}_s + h\right] = \frac{s}{\beta_z}\mathrm{Re}\left\{A' G_{sr} e^{i\vartheta_s}\right\} \tag{3.80}$$

$$\mu \dot{X}' = \frac{1}{\beta_z}\mathrm{Re}\left\{A' G_{sy} e^{i\vartheta_s}\right\} - g_t \mu r_b \cos\phi \tag{3.81}$$

$$\mu \dot{Y}' = -\frac{1}{\beta_z}\mathrm{Re}\left\{A' G_{sx} e^{i\vartheta_s}\right\} - g_t \mu r_b \sin\phi \tag{3.82}$$

Resonant Component of the Waveguide Mode

The normalized amplitude and the axial propagation constant are defined as $A' = eA / m_{e0} c\omega$,

$k = k_z / h$. The Helmholtz equation in the interaction circuit is expressed using a membrane function Ψ, which is given by

$$\nabla_t^2 \Psi + k_t^2 \Psi = 0 \tag{3.83}$$

where, ∇_t^2 is the Laplacian operator in the transverse direction of the circuit and k_t is the transverse propagation constant. The following boundary conditions need to be satisfied

$$\left.\frac{\partial \Psi}{\partial \hat{n}}\right|_{waveguide\ wall} = 0 \text{ , for TE mode and } \quad \Psi\big|_{waveguide\ wall} = 0 \qquad \text{for TM mode} \tag{3.84}$$

where $\hat{n}$ is a unit normal to the waveguide wall. When Ψ is an analytic function it may be represented as

$$\Psi(\vec{r}_t) = \int_0^{2\pi} \hat{\Psi}(u) e^{-ik_t(x\cos u + y\sin u)} du \tag{3.85}$$

It may be mentioned that Ψ need not be a unique function and its periodicity in azimuthal direction 'θ' enables to represent it as a sum of infinite harmonics in the form of

$$\Psi(\vec{r}_t) = \sum_{l=-\infty}^{\infty} \Psi_l e^{il\theta} \tag{3.86}$$

where,
$$\Psi_l = \frac{1}{2\pi} \int_0^{2\pi} \Psi e^{-il\theta} d\theta \tag{3.87}$$

Substituting for Ψ from equation (3.85) in (3.87), we get

$$\Psi_l = \frac{1}{2\pi} \int_0^{2\pi} \left\{ \int_0^{2\pi} \hat{\Psi}(u) e^{-ik_t(x\cos u + y\sin u)} du \right\} e^{-il\theta} d\theta \tag{3.88}$$

Now, let us consider a gyrating electron whose instantaneous positions are given by

$$x = X + r_L \cos\theta \qquad\qquad y = Y + r_L \sin\theta \tag{3.89}$$

The function Ψ_l can now be determined along the unperturbed electron trajectory as

$$\Psi_l = \frac{1}{2\pi}\int_0^{2\pi}\left\{\int_0^{2\pi}\hat{\Psi}(u)e^{-ik_t[(X+r_L\cos\theta)\cos u+(Y+r_L\sin\theta)\sin u]}du\right\}e^{-il\theta}d\theta \tag{3.90}$$

Introducing $\bar{\theta}=\theta-u.$ now, The Ψ_l ca be expressed as

$$\Psi_l = \int_0^{2\pi}\hat{\Psi}(\mathrm{u})e^{-ik_t(X\cos u+Y\sin u)-ilu}du.\frac{1}{2\pi}\int_0^{2\pi}e^{-i[k_t r_L\cos\bar{\theta}+l\bar{\theta}]}d\bar{\theta} \tag{3.91}$$

In the above equation we define

$$\frac{1}{2\pi}\int_0^{2\pi}e^{-i[k_t r_L\cos\bar{\theta}+l\bar{\theta}]}d\bar{\theta}=(-i)^l J_l(k_t r_L) \tag{3.92}$$

and
$$\int_0^{2\pi}\hat{\Psi}(\mathrm{u})e^{-ik_t(X\cos u+Y\sin u)-ilu}du=\left(\frac{1}{-ik_t}\right)^l\left(\frac{\partial}{\partial X}+i\frac{\partial}{\partial Y}\right)\Psi(X,Y) \tag{3.93}$$

where, Ψ is an analytic function with no singularity and J_l is the Bessel function of the first kind of order 'l' with the argument in the parenthesis. Now we define the following quantities

$$\Psi_l = J_l(k_t r_L)L_l(X,Y) \tag{3.94}$$

$$L_l=\frac{1}{k_t}\left(\frac{\partial}{\partial X}+i\frac{\partial}{\partial Y}\right)^l\Psi(X,Y) \tag{3.95}$$

L_l can be identified to be the form factor of the interaction circuit and decides the coupling of the cyclotron wave to the resonant waveguide mode. When 'l' is negative, we get the condition for anomalous Doppler cyclotron resonance

$$\omega\simeq\frac{-|s|\Omega}{1-h\beta_z} \tag{3.96}$$

$$\Psi_{l<0}=J_{|l|}(k_t r_L)L_{|l|}(X,Y) \tag{3.97}$$

where, $$L_{|l|} = \frac{1}{k_t}\left(\frac{\partial}{\partial X} + i\frac{\partial}{\partial Y}\right)^{|l|} \Psi(X,Y) \tag{3.98}$$

Since the gyro-TWT amplifier is operated in transverse electric mode, in the present analysis, only TE modes have been considered. Assuming a time-harmonic response of the form $\sim e^{-i(\omega t - k_z z + n\phi)}$. The field components for *TE* modes can be expressed as

$$E_{sz} = 0 \tag{3.99}$$

$$E_{sr} = i\mu_0 c \frac{k}{k_t^2}\frac{1}{r}\frac{\partial \Psi}{d\phi} \tag{3.100}$$

$$E_{s\phi} = -i\mu_0 c \frac{k}{k_t^2}\frac{\partial \Psi}{dr} \tag{3.101}$$

$$H_{sz} = \Psi \tag{3.102}$$

$$H_{sr} = i\frac{k_z}{k_t^2}\frac{\partial \Psi}{\partial r} \tag{3.103}$$

$$H_{s\phi} = i\frac{k}{k_t^2}\frac{1}{r}\frac{\partial \Psi}{\partial \phi} \tag{3.104}$$

In the above equations and henceforth the suffix *s* in the subscript represents the resonant components of the field and the Lorentz force with the beam cyclotron harmonic. The beam-mode dispersion is governed by

$$\omega - s\frac{\Omega}{\gamma} - k_z v_z \geq 0 \tag{3.105}$$

It is assumed that the interaction is single mode at the resonant harmonic. Using the above field expressions (2.87)–(2.92) on can express the components of the Lorentz force given by

$$\vec{G} = \vec{E} + \vec{v} \times \vec{B} \tag{3.106}$$

as
$$G_r = i\mu_0 c\frac{k}{k_t^2}\frac{1}{r}\left(1-h\beta_z\right)\frac{\partial\Psi}{\partial\theta}+\mu_0 c\beta_t\,\Psi \tag{3.107}$$

$$G_\theta = -i\mu_0 c\frac{k}{k_t^2}\left(1-h\beta_z\right)\frac{\partial\Psi}{dr} \tag{3.108}$$

$$G_z = -i\mu_0 c\frac{k_z}{k_t^2}\beta_t\frac{\partial\Psi}{dr} \tag{3.109}$$

where,
$$\Psi = \sum_{n=-\infty}^{\infty}\Psi_n e^{in\phi} = \sum_{n=-\infty}^{\infty}J_n\left(k_t r_L\right)L_n(X,Y)e^{in\phi} \tag{3.110}$$

Now, we introduce the following normalized parameters $\xi = k_t r_L$, and $\kappa = k_t/k$

and we use
$$\beta_t = \frac{v_t}{c} = \frac{r_L\Omega}{c} \approx \frac{r_L\omega(1-h\beta_z)}{cs} = \frac{\xi}{\kappa}\left(\frac{1-h\beta_z}{s}\right) \tag{3.111}$$

to express the radial component of the Lorentz force as

$$G_r = \sum_{l=-\infty}^{\infty}J_l\left(\xi\right)L_l(X,Y)\mu_0 c\left[\frac{\xi}{\kappa}\left(\frac{1-h\beta_z}{s}\right)-\frac{k}{k_t^2}\frac{l}{r}\left(1-h\beta_z\right)\right] \tag{3.112}$$

To obtain the resonant component we substitute $l = s$ and $r = r_L$ to obtain

$$G_{r,s} = \mu_0 c\frac{1-h\beta_z}{s\kappa}\left[\xi-\frac{s^2}{r}\right]J_s\left(\xi\right)L_s(X,Y) \tag{3.113}$$

Recalling the Bessel equation

$$\frac{d}{d\xi}\left[\xi\frac{d}{d\xi}J_s\left(\xi\right)\right]+\left(\xi-\frac{s^2}{\xi}\right)J_s\left(\xi\right)=0 \tag{3.114}$$

We can rewrite $G_{r,s}$ as

$$G_{s,r} = -\mu_0 c\left(\frac{1-h\beta_z}{s\kappa}\right)\frac{d}{d\xi}\left[\xi\frac{d}{d\xi}J_s\left(\xi\right)\right]L_s(X,Y) \tag{3.115}$$

Similarly, we can write the equations for the other components as

$$G_{s,\theta} = -i\mu_0 c\left(\frac{1-h\beta_z}{\kappa}\right)J_s'(\xi)L_s(X,Y) \tag{3.116}$$

and $$G_{s,z} = -i\mu_0 c\left(\frac{h\beta_t}{\kappa}\right)J_s'(\xi)L_s(X,Y) \tag{3.117}$$

Furthermore, $$\xi = k_t r_L = \kappa k r_L = \kappa\frac{\omega}{c}\frac{v_t}{\Omega} = \kappa\beta_t\frac{\omega}{\Omega} \tag{3.118}$$

Recalling that $s\Omega \approx \omega(1-h\beta_z)$ we can ξ express as

$$\xi \cong \frac{s\kappa}{1-h\beta_z}\beta_t \tag{3.119}$$

For moderate values of β_t corresponding to mildly relativistic beams $\xi \ll 1$, enabling us to expand the Bessel functions as

$$J_s(\xi) \simeq \frac{1}{s!}\left(\frac{\xi}{2}\right)^s \tag{3.120}$$

$$J_s^{'}(\xi) \simeq \frac{1}{2(s-1)!}\left(\frac{\xi}{2}\right)^{s-1} \tag{3.121}$$

$$\frac{\partial}{\partial\xi}\xi J_s^{'}(\xi) \simeq \frac{s}{2(s-1)!}\left(\frac{\xi}{2}\right)^{s-1} \tag{3.122}$$

Using the previous result we can simplify $(3.115)-(3.117)$

$$G_{s,r} \simeq -\mu_0 c\left(\frac{1-h\beta_z}{s\kappa}\right)\frac{1}{2(s-1)!}\left(\frac{\xi}{2}\right)^{s-1}L_s\left(X,Y\right) \tag{3.123}$$

$$G_{s,\theta} \cong -i\mu_0 c\left(\frac{1-h\beta_z}{\kappa}\right)\frac{1}{2(s-1)!}\left(\frac{\xi}{2}\right)^{s-1}L_s\left(X,Y\right) \tag{3.124}$$

$$G_{s,z} \cong -i\mu_0 c\frac{h}{\kappa}\beta_t\frac{1}{2(s-1)!}\left(\frac{\xi}{2}\right)^{s-1}L_s(X,Y) \tag{3.125}$$

It is interesting to note that $G_{s,\theta} = -iG_{s,r}$. In a similar manner we can also derive the expressions for $G_{s,x}$ and $G_{s,y}$.

After determining the resonant components of Lorentz force, equation for the evolution of electron energy along the interaction circuit is formulated as

$$\varepsilon = \gamma m_{e0} c^2 \tag{3.126}$$

The time rate of change of energy is given by

$$\frac{d\varepsilon}{dt} = -e\left(\vec{v}_t . \vec{E}_\theta\right) \tag{3.127}$$

which may be further simplified and expressed in terms of the normalized variables as

$$\frac{d\gamma}{dz'} = -\left(\frac{\vec{p}}{p_z} . \frac{e\vec{E}}{m_{e0} c\omega}\right) \tag{3.128}$$

Using $\vec{p}.\vec{E} = p_\phi E_{s\phi}$ we finally obtain

$$\frac{d\gamma}{dz'} = -i\frac{p'_t}{p'_z}\frac{\mu_0 c}{\kappa} J'_s(\xi)\,\mathrm{Re}\left\{A' L_s\left(X,Y\right)e^{i\vartheta_s}\right\} \tag{3.129}$$

From the expression for $\dot{p}'_z$ in (3.80) we obtain

$$\frac{dp'_z}{dz'} = \mu_0 c\frac{h}{\kappa}\frac{\beta_t}{\beta_z}\,\mathrm{Re}\left\{iA' J'_s(\xi) L_s\left(X,Y\right)e^{i\vartheta_s}\right\} \tag{3.130}$$

from the expression for in $\dot{p}'_t$ (3.79) we get

$$\frac{dp'_t}{dz'} = \mu_0 c\frac{1-h\beta_z}{\kappa\beta_z}\,\mathrm{Re}\left\{iA' J'_s(\xi) L_s\left(X,Y\right)e^{i\vartheta_s}\right\} \tag{3.131}$$

and finally from the expression $\dot{\vartheta}_s$ in (3.81) we get

$$p'_t\left(\dot{\vartheta}_s + \frac{1-h\beta_z - s\mu/\gamma}{\beta_z}\right) = -\mu_0 c\;\frac{1-h\beta_z}{\kappa\beta_z}\;\left(\frac{d}{d\xi}\xi J'_s(\xi)\right)\mathrm{Re}\left\{A' L_s\left(X,Y\right)e^{i\vartheta_s}\right\} \tag{3.132}$$

One may also derive (3.129) using $\gamma^2 = 1 + p_t'^2 + p_z'^2$,

$$\frac{d\gamma}{dz'} = \frac{1}{\gamma}\left(p_t' \frac{dp_t'}{dz'} + p_z' \frac{dp_z'}{dz'} \right) \quad , \tag{3.133}$$

(3.130), and (3.131). It is interesting to note that if the terms due to $\vec{R}_r$ and $\vec{R}_\theta$, originating from the radial component of the magnetic field, are substituted into the RHS of the equation (3.133) one discovers that there is no net change in γ. This is intuitively obvious, as a DC magnetic field cannot contribute to the energy of the charged particle. It however, does change the distribution of the energy between the transverse and longitudinal directions as is evident from the terms containing g in (3.79) and (3.80). In the limit of very low in homogeneity in the magnetic field the above equations conserve the adiabatic constant of the electron motion.

Now defined a normalized energy parameter as

$$w = \frac{2(1 - h\beta_{z0})}{\beta_{t0}^2} \frac{\gamma_0 - \gamma}{\gamma} \tag{3.134}$$

and changes in the longitudinal momentum of the electron or absorbing photons.

$$b = \frac{h\beta_{t0}^2}{2\beta_{z0}(1 - \mathrm{h}\,\beta_{z0})} \tag{3.135}$$

Now, the derivative of w is expressed with respect to normalized distance and after simplifying we obtain

$$\frac{dw}{dz'} = 2i \frac{(1-w)^{s/2}}{(1-bw)} \mathrm{Re}\left\{ \mathcal{F} e^{i\vartheta_s} \right\} \tag{3.136}$$

where

$$\mathcal{F} = \frac{\mu_0 c}{\kappa} \frac{1-h\beta_{z0}}{\gamma_0 \beta_{t0} \beta_{z0}} \frac{1}{2^s (s-1)!} \left(\frac{\kappa p'_{t0}}{\mu} \right) A' L \tag{3.137}$$

and

$$p'_t \left(\dot{\vartheta}_s + \frac{1-h\beta_z - s\mu/\gamma}{\beta_z} \right) = -\mu_0 c \frac{1-h\beta_z}{\kappa \beta_z} \left(\frac{d}{d\xi} \xi J'_s(\xi) \right) \mathrm{Re}\left\{ A' L_s(X,Y) e^{i\vartheta_s} \right\} \tag{3.138}$$

In the previous sections, the self consistent EM fields in the interaction circuit and the equations governing the evolution of the phase and energy of electrons as a function of the field amplitude have been formulated. The obvious final step in this analysis is to express the amplitude of the self-consistent field in terms of a practical quantity, namely, the beam current which is written for a thin annular electron beam streaming through a cylindrical waveguide.

$$\iint dS_\perp \, j_{z0} = -|I_0| \tag{3.139}$$

where, I_0 is the DC beam current. The coupling between electrons and the RF field is decided by the coupling factor, $L_s(X,Y)$ as represented in (3.98). Substituting (3.139) into (3.46) we obtain

$$\frac{dA(z)}{dz} = \frac{|I_0|}{N_s} \frac{1}{\pi} \int_0^{2\pi} \frac{\vec{j}_t . \vec{E}_s}{j_z} e^{i(\omega t - k_z z)} d(\omega t_0) \tag{3.140}$$

where, we have assumed $(\Delta k_z) \approx 0$. The electric field in the above equation can be expressed as a sum of Fourier components in the form

$$\vec{E}_s^* e^{i(\omega t - k_z z)} = \sum_{l=-\infty}^{\infty} \vec{E}_{s,l}^* e^{i(\omega t - k_z z - l\theta)} \tag{3.141}$$

For

$$\vartheta_s = s\theta - (\omega t - k_z z) \tag{3.142}$$

we obtain

$$\frac{dA(z)}{dz} = \frac{|I_0|}{N_s} \frac{1}{\pi} \int_0^{2\pi} \frac{\vec{p}_t . \vec{E}^*_{s,s}}{p_z} e^{-i\vartheta_s} d\phi_0 \tag{3.143}$$

Substituting the expression for $\vec{E}^{*}_{s,s}$ we obtain

$$\frac{dA(z)}{dz} = -\frac{i}{\pi}\frac{|I_0|}{N_s}\frac{c\mu_0}{\kappa}\frac{p_{t0}}{p_{z0}}\frac{L^{*}_{s}}{2^s(s-1)!}\left(\frac{\kappa p'_{t0}}{\mu}\right)^{s-1}\int_0^{2\pi}\frac{(1-w)^{s/2}}{(1-bw)}e^{-i\vartheta_s}d\vartheta_0 \tag{3.144}$$

Making transition from $dA(z)/dz$ to $dA'(z)/dz$ and replacing $A'(z)$ by $\mathcal{F}$ from (3.137), we finally get

$$\frac{d\mathcal{F}(z)}{dz'} = -iI'_0\frac{1}{2\pi}\int_0^{2\pi}\frac{(1-w)^{s/2}}{(1-bw)}e^{-i\vartheta_s}d\vartheta_0 \tag{3.145}$$

where, the normalized current parameter is given by

$$I'_0 = \frac{2e|I_0|\mu_0^2}{\gamma_0 m_{e0}N_s}\frac{(1-h\beta_{z0})}{k_t^2\beta_{z0}^2}\left(\frac{1}{2^s(s-1)!}\right)^2\left(\frac{\kappa p'_{t0}}{\mu}\right)^{2(s-1)}|L_s|^2 \tag{3.146}$$

The whole interaction process can now be represented by the following set of equations (3.136), (3.132) and (3.145) connecting the electron energy, phase and the field amplitude in a self-consistent setup [Sirigiri (1999)]. We rewrite these equations below

$$\frac{dw}{dz'} = 2\frac{(1-w)^2}{(1-bw)}\mathrm{Im}\left\{\mathcal{F}e^{i\vartheta_s}\right\} \tag{3.147}$$

$$\frac{d\vartheta_s}{dz'} = \frac{1}{(1-bw)}\left[\bar{\mu}w - \bar{\Delta} + s(1-w)^{s/2-1}\,\mathrm{Re}\left\{\mathcal{F}e^{i\vartheta_s}\right\}\right] \tag{3.148}$$

$$\frac{d\mathcal{F}}{dz'} = -iI'_0\frac{1}{2\pi}\int_0^{2\pi}\frac{(1-w)^{s/2}}{(1-bw)}e^{-i\vartheta_s}d\vartheta_0 \tag{3.149}$$

where $\bar{\Delta} = \Delta/\beta_{z0}$. The field inside the interaction circuit is expressed in membrane function

$$\Psi^{\pm}_{mn} = C_{mn}J_m(k_t r_w)e^{\pm jm\theta} \tag{3.150}$$

where, θ is the azimuthal angle, 'r_w' is the radius of the interaction circuit and C_{mn} is the normalization parameter and for the transverse electric $\left(TE_{mn}\right)$ mode of operation which is defined as

$$C_{mn} = \left\{\sqrt{\pi\left(k_t^2 r_w^2 - m^2\right)} J_m\left(k_t r_w\right)\right\}^{-1} \tag{3.151}$$

Substitute equations (3.99) - (3.104) ,the form factor can be obtained as

$$L_{|s|} = C_{mn} J_{s\pm m}\left(k_t r_b\right) \tag{3.152}$$

It is very essential to define the coupling factor which is given by

$$\text{Coupling Factor} = \frac{\left|L_s^2\right|}{N_s} \tag{3.153}$$

The power propagating along the interaction circuit is given by

$$P = \frac{1}{2}\text{Re}\left\{\iint\left(\vec{E}_s \times \vec{H}_s^*\right) dS_\perp\right\} = 8\mu_0 c C_{mn}^2 k k_z / k_t^4 \tag{3.154}$$

The corresponding electronic efficiency of gyro-TWT amplifier is defined as

$$\eta_e = \frac{\beta_{to}^2}{2\left(1-1/\gamma\right)\left(1-h\beta_{z0}\right)}\eta_\perp \tag{3.155}$$

where, $\eta_\perp$ is the orbital efficiency which characterizes the changes in the electron orbital momentum in the interaction mechanism.

A computer code for gyro-TWT has been developed and used for analyzing the interaction, i.e., Large Signal Analysis (LSA), based on the single particle analysis. The main focus was on the solving of the coupled equations using numerical techniques. Finally, the 5-6*th* order Runge-Kutta was the best suited method to solve the equations.

3.4.3. *Algorithm for LSA of Gyro-TWT Amplifier*

1. Input the parameters.
2. Compute the required parameters.
3. Input the no. of electrons and divide all the electrons into m different velocity class.
4. Initialize the initial values of energy of all electrons as zero.
5. Initial phase of all the electrons are distributed from 0 to 2π for each velocity class.
6. Solve the three non-linear equations using 5-6^{th} order Runge-Kutta-Vernar numerical technique and store the data generated in each run into an array.
7. Repeat the same process for each electron into different velocity class.
8. Plot the data stored into an array with respect to axial position and energy and phase profile of all the electrons can be seen.
9. Now take the square root of the data generated for field amplitude and this will be the output power profile.

In gyro-TWT, the electrons were divided in different velocity class and phase was distributed from 0 to 2π in each velocity class. The data stored in the data arrays is used to get the customized plot for energy and phase distribution of all the electrons. The output power profile, efficiency, gain etc. can be plotted with the help of the data generated for field profile. Fig. 3.7 depicts the flow chart for the performance estimation of gyro-TWT amplifier. Fig. 3.8 elucidated the schematic diagram of the heavily loaded RF interaction circuit of W-band gyro-TWT amplifier. First 12.0cm of 14.5cm long interaction circuit has been loaded with a resistive material. Loaded linear taper length is 1cm and remaining 2.5cm section is unloaded.

3.4.4. Flow-chart for LSA of Gyro-TWT Amplifier

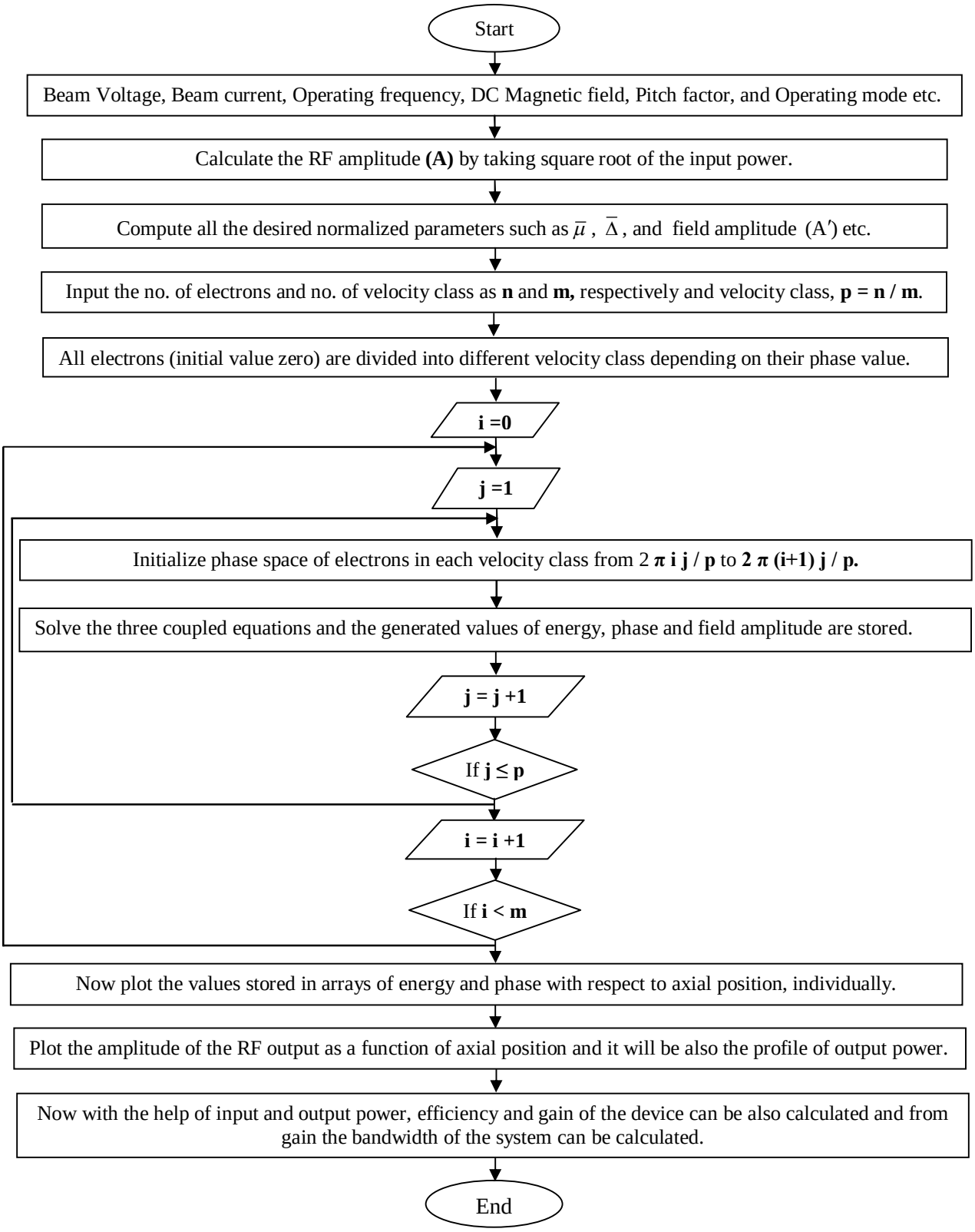

Figure 3.7. Flow chart for the performance estimation of gyro-TWT amplifier.

3.5. Numerical Benchmarking

The generalized single particle time independent analysis presented in the section 3.4 are further exploited numerically to observe the gyro-TWT amplifiers behaviour with the aid of computer friendly computations. To validate the developed analytical model, W-band gyro-TWT amplifier experiments reported in the literature have been selected [Song *et al.* (2004)]. This performance estimation has been carried for the numerical benchmarking the code, so that they can be successfully implemented for the design and analysis of the gyro-TWT amplifier. Table 3.1 shows the design specifications taken for analysis of 92GHz gyro-TWT.

The dispersion diagram of the W-band gyro-TWT amplifier for the desired TE_{01} mode at fundamental harmonic operation has been shown in Fig. 3.9(a) and there is certain finite width of unstable region on the intersection of the beam mode and the desired *TE* waveguide mode. If this unstable region is confined to the forward wave region ($k_z > 0$) only then the RF wave will travel down the interaction circuit with convectively growing amplitude.

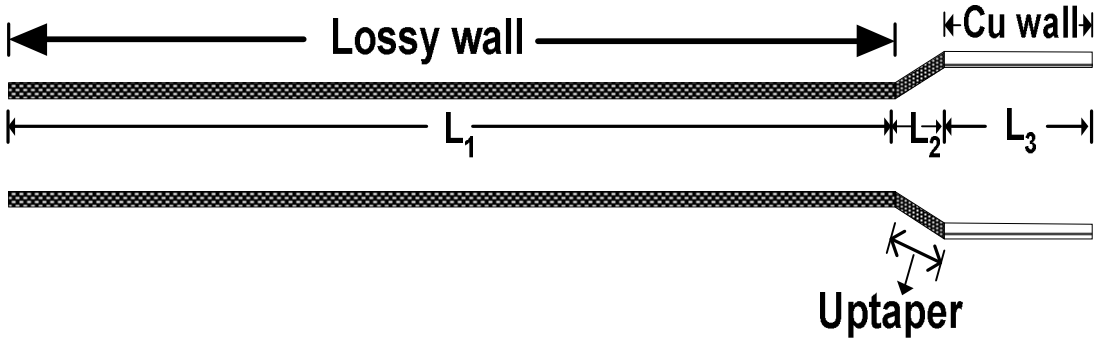

Figure 3.8. Schematic diagram of the uniformly loaded RF interaction circuit of W-band gyro-TWT amplifier.

Table 3.1 Design specifications for 92GHz, 140kW gyro-TWT amplifier [Song *et al.* (2004)]

Parameters	**Spectfication**
Voltage	100kV
Current	5A
pitch factor	1.0
Operating mode	TE_{01}
Velocity spread	5%
Magnetic field, B_0	35.6kG
B_0/B_g	0.995
Cutoff frequency	91.0GHz
Lossy wall resistivity	$70{,}000\rho_{Cu}$
Guiding center radius	$0.45r_w$
Circuit radius, r_w	0.201cm
Lossy circuitlength, L_1	11.0cm
Loss taper length, L_2	1.0cm
Copper circuit length, L_3	2.5cm
Total circuit length	14.5cm

However, if the cyclotron harmonic beam-wave synchronism lines cross in the region where the propagation constant is negative ($k_z < 0$), which generates an internal feedback route and thereby the backward wave oscillation is generated. In addition, the grazing intersection point is chosen as an operating point in order to achieve high gain, which is at near cut-off as shown in Fig. 3.9 (a). As the beam current is large enough, the unstable spectrum extends into backward-wave region which cause convective instability transitions into absolute instability. The coupling coefficient between the electron beam and RF fields in the cylindrical waveguides is defined as,

$$C_{mn} = \frac{J_{m\pm s}^2(k_\perp r_b)}{(\nu_{mn}^2 - m^2)J_m^2(\nu_{mn})} \qquad (3.156)$$

Using this expression, the optimum radius of the electron beam can be determined for the maximum coupling to the chosen mode. The normalized coupling coefficient (C_{mn}) of TE_{01} mode gyro-TWT amplifier and competing modes with respect to the normalized beam radius for the different number of modes $(TE_{11}^1, TE_{21}^1, TE_{01}^1$ and $TE_{02}^2)$ is shown in Fig. 3.9 (b). Fig. 3.9 (b) clearly indicates peak value of coupling coefficient for the desired mode at $r_b / r_w = 0.45$.

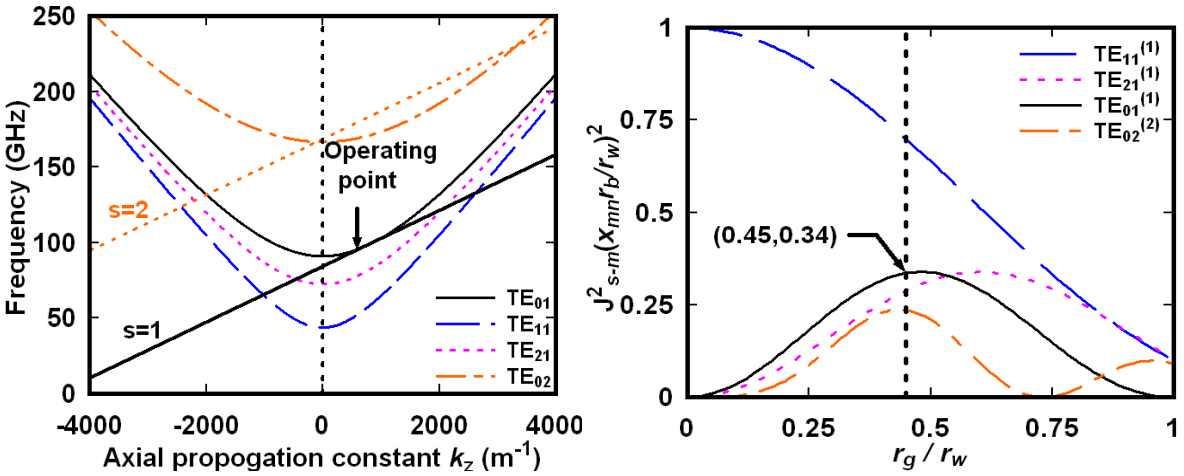

Figure 3.9. (a) Dispersion diagram for operating TE_{01}^1 and possible oscillating modes for the loaded gyro-TWT amplifier, and **(b)** Dependence of gyro-TWT coupling co-efficient on the guiding radius for desired and competing modes.

Figure 3.10 shows the spatial power growth of the RF power with 5% velocity spread. The self-consistent nonlinear code was modified then employed to evaluate the large signal characteristics. Figure 3.10 clearly indicate for a given parameter saturated output power 144.4kW for a velocity spread of 5%.

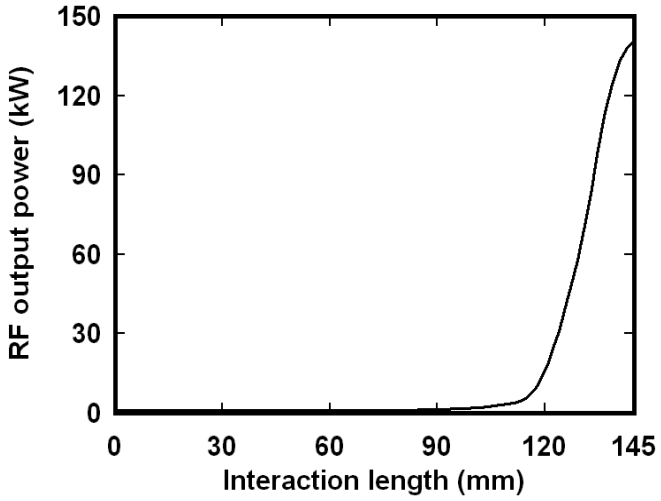

Figure 3.10. Spatial power growth of the TE_{01}^{1} with 5% velocity spread of W-band gyro-TWT amplifier.

Figure 3.11(a) shows the variation of RF output power and efficiency with pitch factor. Figure3.11 (a) clearly indicates that the device output is sensitive with the variation of pitch factor and yield maximum power 144.4kW and gain 28.9% when the pitch factor is unity. Figure 3.11(b) elucidates the variation of output power, efficiency and gain with drive signal frequency. Fig. 3.11(b) clearly indicates that maximum output power 144.4kW with 28.9% efficiency, 5.2% bandwidth, and 50.1dB saturated gain for a velocity spread of 5%. Figure 3.12(a) shows the variation of energy of electrons and describe the modulation of momentum of particles along the propagation direction in the interaction circuit. Due to phase bunching of electrons in each velocity class, the energy exchange taking place. Due to the interaction between the streaming electrons and the RF signal at the same time energy distribution of electrons changes. At the output, the net energy of electron is negative which depict that electrons transferred their energies to the wave. The bunching of all the particles exists in the nearly middle of the interaction circuit. Once electrons transferred their energy to wave, the de-bunching takes place.

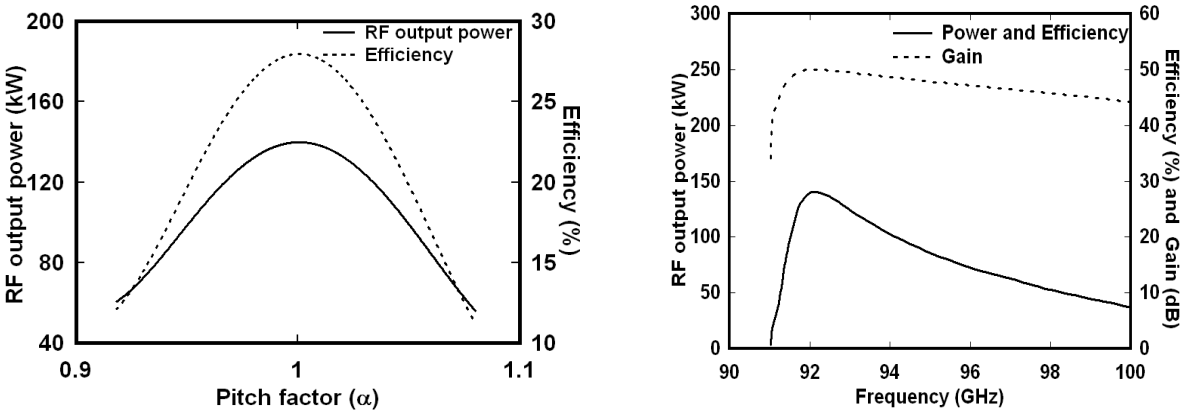

(a) **(b)**

Figure 3.11(a). Variation of RF output power and efficiency with pitch factor and (b) Variation of power output, gain, and efficiency with respect to input frequencies.

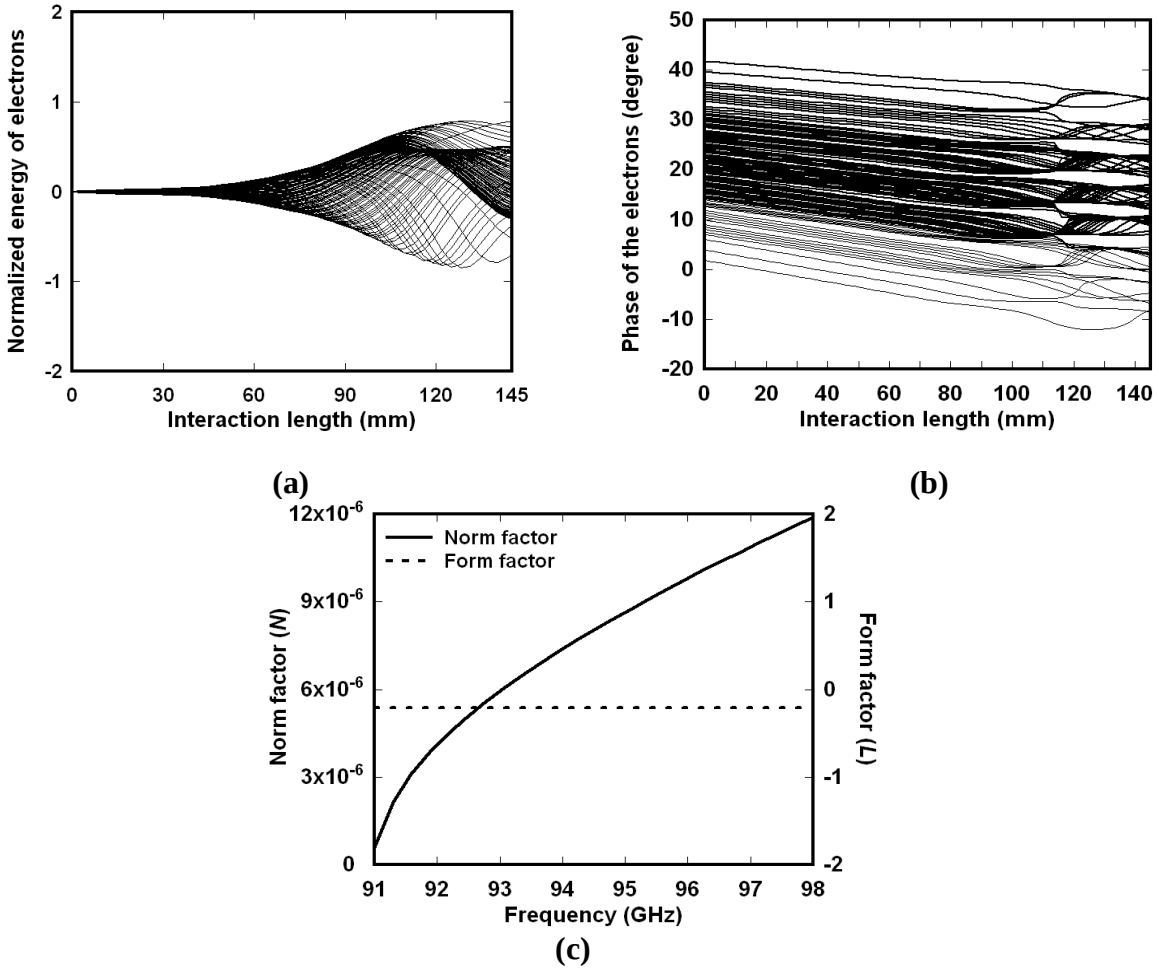

(a) **(b)**

(c)

Figure 3.12(a). Energy of electrons along length of the interaction circuit, **(b)** Phase variation of electrons along length of the interaction circuit for 5% velocity spread, and **(c)** Variation of Norm factor and Form factor with frequency.

Figure 3.12(b) illustrates the phase variation of electrons along the propagation direction of the interaction circuit for 5% velocity spread. Due to cyclotron resonance mismatch electron slippage with respect to the electromagnetic field. This makes a difference in the axial velocity of the beam, which in turn affect the performance of the gyro-TWT amplifier. We have considered the velocity spread as a Gaussian distribution and in which the same velocity sets of electrons are grouped together. Each of these sets is described by the weight of the Gaussian distribution and the total number of macro electrons and every velocity set has the same initial longitudinal and transverse momentum. The initial phase of electrons within each velocity set is uniformly distributed over the interval 0 to 2π and also to avoid the overlapping between different velocity sets of electrons, we have divided the phase space for each set from $2n\pi$ to $2(n+1)\pi$.

Figure 3.12(c) shows the variation of norm factor and form factor with frequency. The form factor (L_s) refers the coupling between the cyclotron wave and the resonant waveguide mode. Form factor depends on the transverse dimension of the waveguide and operating mode but not frequency dependent, as a result for all operating frequencies, the value of form factor will remain same as shown in Fig. 3.12(c). The norm factor (N_s) which describes the RF power propagating through the interaction circuit per unit area, is dependent on both operating mode and frequency. This increases as the operating frequency increases, as can be seen from Fig. 3.12(c).

3.6. Conclusion

In this chapter, the time-independent single particle analysis for the CRM single-mode interaction which is derived from the basic principles of kinetic approach has been developed. The nonlinear interaction can be described by self-consistent equations given by

eqns. (3.147) - (3.149) . For validation, nonlinear analysis is carried out through the numerical code with the aid of "MATLAB".A good matching with the reported experimental results [Song *et al.* 2004] for a given output parameters has been observed. The electron beam velocity spread always present practical device because of the non-uniform electrons emission from a real cathode due to practical constraints, like, non-uniform heating of cathode, cathode surface roughness, and electrons repulsions due to space charge. 2% to 5% electron velocity spreads are usually found in the practical devices and this degrades the tube performance, both RF output power and efficiency. The nonlinear analysis is modified to include this effect by making the normalized parameters: field amplitude, momentum and electron phase terms velocity dependent. This heavily loaded W-band gyro-TWT operating in the fundamental harmonic TE_{01} mode, yielded 144.4kW saturated output power with 5% bandwidth, 28.9% efficiency and 50.1dB saturated gain for 5% velocity spread, when the 100kV, 5A electron beam with unity pitch factor is applied. The effects of the various parameters, such as, variations in the pitch factor, microwave input RF frequency, norm factor, form factor, bandwidth and RF output power are explored and discussed. This sensitivity studies will help this device developer to analyse their device under practical conditions. A very important obstacle for the performance of gyro-TWT is spontaneous oscillation. Magnetic field requirement is directly proportional to operating frequency. For fundamental harmonic operation, strong DC magnetic field is required, so in order to reduce the magnetic field requirement higher harmonic interaction is preferred.

In the next chapter, PIC simulation of Ka and W-band fundamental harmonic gyro-TWT amplifier is carried out. The mode competition is studied by considering the competing modes along with the operating mode.